The Effect of Front and Rear Surface Recombination Velocities on the Photocurrent of Buried Emitter Silicon Solar Cell

Sayantan Biswas[*], Ashim Kumar Biswas[*] and Amitabha Sinha[*‡]

*Department of Physics, University of Kalyani, Kalyani-741235, West Bengal, India.

(sayan.solar@gmail.com, kumarashimbiswas@gmail.com, asinha333@gmail.com)

‡Corresponding Author; Amitabha Sinha, Department of Physics, University of Kalyani, Kalyani-741235, West Bengal, India. Tel: +919330951068, asinha333@gmail.com.

Received: *28.04.2015* Accepted: *14.06.2015*

Abstract- Analytical work on the buried emitter solar cell (BESC) has been carried out based on the model presented previously by various researchers. The minority carrier distribution and the photocurrent contribution from the front region and also the rear region of the cell have been studied, taking into consideration the effects of front surface and rear surface recombination velocities. It is observed from these theoretical studies that by reducing these recombination velocities, there is significant improvement in the photocurrent contributions from these regions. This emphasizes the role of a back surface field (BSF) in such devices. It may be mentioned here that in some recent experimental studies on new types of BESC structures, heavily doped BSF regions have been included by investigators.

Keywords- Buried emitter silicon solar cell; surface recombination velocity; photocurrent; minority carrier concentration.

1. Introduction

Ever since the reporting of the first silicon solar cells [1-2], lot of research work has been done on these cells during the last few decades [3-6]. Efforts have been made to improve the efficiency of the solar cells and various modified structures have been developed, which resulted in improved efficiency. A new model of high efficiency buried emitter silicon solar cell was suggested by Bouazzi et al. [7] in which they carried out analytical work on such cells. The concept of buried emitter structure was discussed by Harder et al. [8], in which they presented experimental results also. Further research work on such structures is discussed by Mertens et al. [9]. Device simulation and analytical model calculation of the buried emitter solar cell (BESC) has been carried out by Harder et al. [10] , where they reported that high efficiency can be achieved by passivating the entire surface of p-type emitters by an oxidised n-type surface layer. In our present paper, the model of Bouazzi et al. [7] is followed and analytical derivations have been carried out for the minority carrier distribution and the photocurrent contributions from the front and rear regions of the BESC structure. In addition, we have also taken into account the effects of heavy doping in these regions and have obtained the values of diffusion constant, mobility, lifetime and diffusion length in these regions based on research work reported by various researchers.

2. Analysis

The schematic diagram of a buried emitter solar cell considered by Bouazzi et al. [7] is shown in Fig.1.

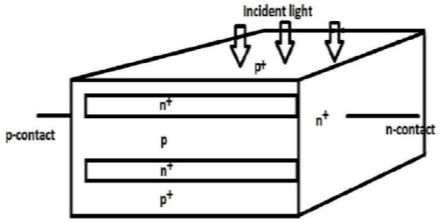

Fig. 1. Schematic diagram of a buried emitter solar cell.

There are five layers, p^+ n^+ p n^+ p^+. At each junction, there is a space charge region. The co-ordinates to be used in the analysis are shown in Fig.2. The mathematical approach to develop the analytical expressions of photocurrent of the solar cell is discussed here in brief.

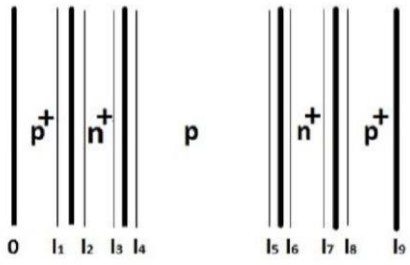

Fig. 2. The coordinates of the solar cell.

Assuming uniform doping in each region, the current density equation for holes and electrons may be written as

$$J_p = -qD_p \frac{dp_n}{dx} \quad (1)$$

and

$$J_n = qD_n \frac{dn_p}{dx} \quad (2)$$

where D_p and D_n are the diffusion constants for holes and electrons respectively and q is the charge of electron.

The continuity equation for minority carrier holes in the n-region is given by

$$G(x) - \frac{p_n}{\tau_p} - \frac{1}{q}\frac{dJ_p}{dx} == 0 \quad (3)$$

and the continuity equation for minority carrier electrons in the p–region is given by

$$G(x) - \frac{n_p}{\tau_n} + \frac{1}{q}\frac{dJ_n}{dx} = 0 \quad (4)$$

where G(x) is the generation rate for electron-hole pairs due to photon absorption.

$$G(x) = F(\lambda)\alpha(\lambda)\, exp[-\alpha(\lambda)x] \quad (5)$$

Combining these equations, the expression for excess minority carrier distribution in each region may be obtained by using suitable boundary conditions at each side of all the five regions of the buried emitter solar cell. Taking the derivative of the excess carrier concentration, at the edge of the depletion region in each junction, the expression for photocurrent may be obtained corresponding to each region. The method used by Bouazzi et al. [7] is followed here to obtain the desired expressions.

The boundary conditions used at various surfaces and at the depletion layer edges of the junctions are as follows

1. At x=0 , $qD_n \frac{dn_p}{dx} = qn_pS_f$

where S_f is the front surface recombination velocity.

2. At x=l_1 , $n_p = 0$
3. At x=l_2 , $p_n = 0$
4. At x=l_3 , $p_n = 0$
5. At x=l_4 , $n_p = 0$
6. At x=l_5 , $n_p = 0$
7. At x=l_6 , $p_n = 0$
8. At x=l_7 , $p_n = 0$
9. At x=l_8 , $p_n = 0$
10. At x=l_9 , $-qD_n \frac{dn_p}{dx} = qn_pS_r$

where S_r is the surface recombination velocity at the rear of the cell.

It may be mentioned here that x = l_1, l_2, l_3, l_4, l_5, l_6, l_7 and l_8 correspond to the depletion layer edges of the various junctions. Since the built in electric fields exist at these depletion layer edges, the excess minority carriers are swept across these junctions and the net concentration of excess holes p_n becomes equal to zero and that of excess electrons n_p becomes equal to zero at the respective junctions .

3. Results and Discussion

The minority carrier electron concentration in the front p - region is given by

$$n_p = \left[\frac{\alpha F L_n^2}{D_n(\alpha^2 L_n^2 - 1)}\right] \times \left[\frac{\left(\alpha L_n + \frac{L_n S_f}{D_n}\right) sinh\left(\frac{l_1 - x}{L_n}\right) + exp(-\alpha l_1)\left\{\frac{L_n S_f}{D_n} sinh\left(\frac{x}{L_n}\right) + cosh\left(\frac{x}{L_n}\right)\right\}}{cosh\left(\frac{l_1}{L_n}\right) + \frac{L_n S_f}{D_n} sinh\left(\frac{l_1}{L_n}\right)} - exp(-\alpha x)\right] \quad (6)$$

And the corresponding photocurrent is [7]

$$J_{n_1} = \left[\frac{q\alpha F L_n}{(1 - \alpha^2 L_n^2)}\right] \times \left[\alpha L_n \exp(-\alpha l_1) + \frac{\left(\alpha L_n + \frac{L_n S_f}{D_n}\right) - \exp(-\alpha l_1)\left\{\frac{L_n S_f}{D_n}\cosh\left(\frac{l_1}{L_n}\right) + \sinh\left(\frac{l_1}{L_n}\right)\right\}}{\cosh\left(\frac{l_1}{L_n}\right) + \frac{L_n S_f}{D_n}\sinh\left(\frac{l_1}{L_n}\right)}\right] \quad (7)$$

Similarly, the calculation for the photocurrent contribution of the other regions has been also performed. The expression for the minority carrier electron concentration from the last p-region of the solar cell may be derived, which is

$$n_p = \left[\frac{\alpha F L_n^2}{D_n(\alpha^2 L_n^2 - 1)}\right] \times \left[\frac{exp(-\alpha l_8)\left\{\frac{L_n S_r}{D_n} sinh\left(\frac{l_9 - x}{L_n}\right) + cosh\left(\frac{l_9 - x}{L_n}\right)\right\} + exp(-\alpha l_8)\left\{\left(\frac{L_n S_r}{D_n} - L_n\alpha\right) sinh\left(\frac{x - l_8}{L_n}\right)\right\}}{\frac{L_n S_r}{D_n} sinh\left(\frac{l_9 - l_8}{L_n}\right) + cosh\left(\frac{l_9 - l_8}{L_n}\right)} - exp(-\alpha x)\right] \quad (8)$$

and the expression for the photocurrent component due to the rear p-region of the cell is given by [7]

$$J_{n_9} = \left[\frac{qF\alpha L_n \exp(-\alpha l_8)}{(\alpha^2 L_n^2 - 1)}\right] \times \left[\alpha L_n + \frac{\left(\frac{L_n S_r}{D_n} - \alpha L_n\right)\exp\{\alpha(l_8 - l_9)\} + \left\{\left(1 - \frac{L_n S_r}{D_n}\right)\exp\left(\frac{l_8 - l_9}{L_n}\right)\right\}}{\frac{L_n S_r}{D_n}\sinh\left(\frac{l_9 - l_8}{L_n}\right) + \cosh\left(\frac{l_9 - l_8}{L_n}\right)} - 1\right] \quad (9)$$

Based on the analysis of the buried emitter solar cell presented above, calculations were performed to study the contributions of the front and rear portions of the solar cell. Using equation (6), the excess minority carrier electron concentration has been calculated and the results have been plotted in Fig.3 for various values of front surface recombination velocity S_f. It is observed that the minority carrier concentration is much higher near the surface, for the cases of low front surface recombination velocities, whereas its value falls significantly for lower values of S_f. For these low values of S_f, many minority carriers are lost at the front surface due to recombination.

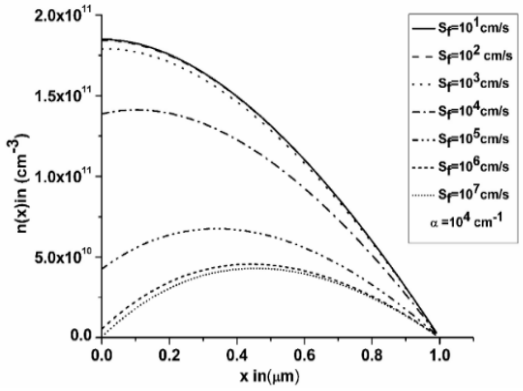

Fig. 3. Variation of excess minority carrier concentration with distance from the front surface corresponding to the different values of surface recombination velocity S_f.

The plot of excess electron density distribution in the front region as a function of absorption coefficient α is given in Fig.4. It is noted that the magnitude of excess carrier concentration increases for increasing values of absorption coefficient α. Since most of the wavelengths corresponding to higher values of α are observed in the front region, the excess carrier concentrations increase for these cases.

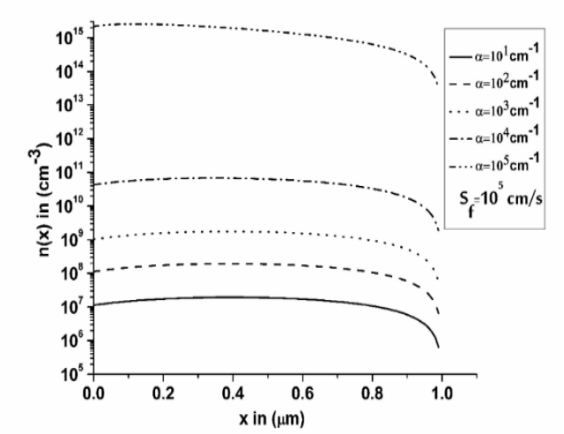

Fig. 4. Variation of excess minority carrier concentration with distance from the front surface corresponding to the different values of absorption coefficient α.

Using equation (7), the photocurrent contribution due to the front region has been calculated. Fig.5 shows the plot of $\frac{J_{nl_1}}{qF}$ versus absorption coefficient α for different values of front surface recombination velocity S_f and the plot of $\frac{J_{nl_1}}{qF}$ versus wavelength is shown in Fig.6 for various values of S_f. It is observed that as the front surface recombination is decreased, the photocurrent contribution from the front layer increases. This is interpreted from the fact that decrease in S_f corresponds to lower recombination at the front surface, which results in increased value of photocurrent contribution from the front layer.

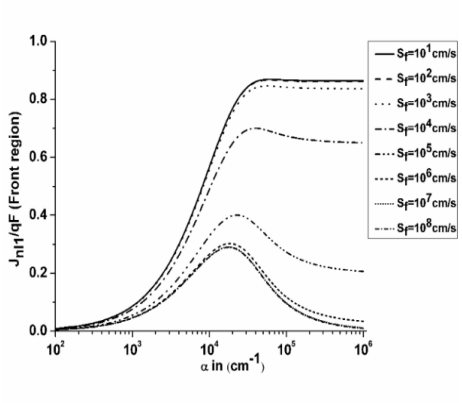

Fig. 5. Variation of $\frac{J_{nl_1}}{qF}$ with absorption coefficient α corresponding to the different values of recombination velocity S_f.

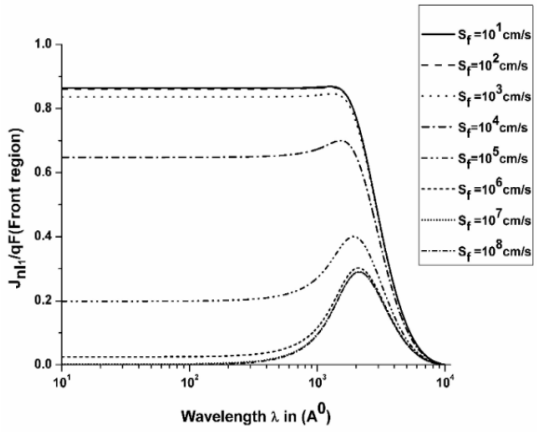

Fig. 6. Variation of $\frac{J_{nl_1}}{qF}$ with wavelength of the incident light corresponding to the different values of recombination velocity S_f.

Similarly, using equation (8) the minority carrier concentration in the back region of the cell has been calculated and the corresponding photocurrent contribution due to this region has been obtained from equation (9). The plot of minority carrier distribution in the back region of the solar cell as a function of position has been given in Fig.7

corresponding to different values of rear surface recombination velocity S_r, and the same plot as a function of absorption coefficient α is shown in Fig.8. From Fig.7 it is observed that there is a large concentration of excess minority carrier near the rear surface for smaller values of S_r. Since in this case, low recombination at the back leads to larger accumulation of carriers there. It is observed from Fig.8 that maximum carrier concentration is obtained for value of absorption coefficient α of about $10^2 cm^{-1}$. For α $=10^3 cm^{-1}$ the plot of excess minority carrier electrons concentration almost coincides with the x-axis.

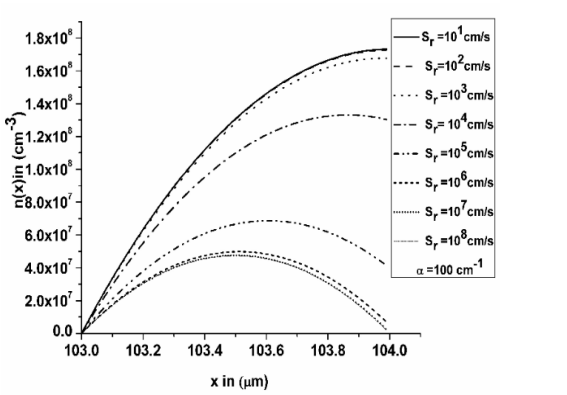

Fig. 7. Variation of minority carrier concentration with distance at the rear region corresponding to the different values of surface recombination velocity S_r.

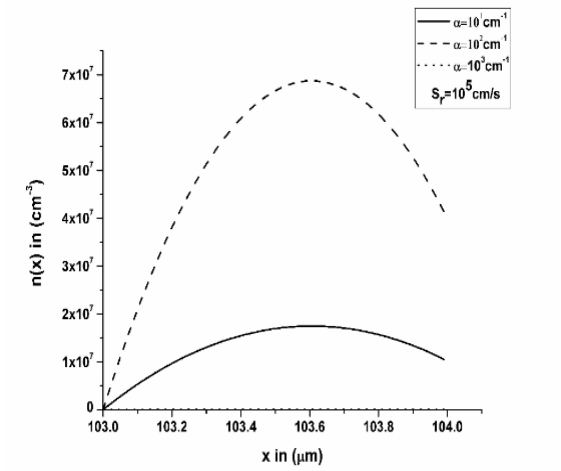

Fig. 8. Variation of minority carrier concentration with distance at the rear region corresponding to the different values of absorption coefficient α.

Fig. 9 shows the variation of $\frac{J_{nl_2}}{qF}$ as a function of α for different values of S_r and Fig.10 shows the plot of $\frac{J_{nl_2}}{qF}$ as a function of wavelength λ for various values of S_r. It is observed from these figures that though the contribution to the overall photocurrent from this layer is much smaller than that from the front layer, it is still dependent significantly on the rear surface recombination velocity.

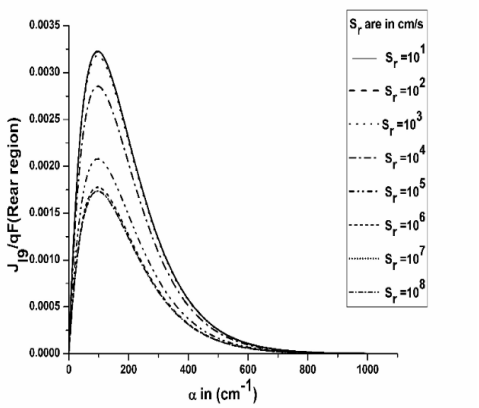

Fig. 9. Variation of $\frac{J_{nl_2}}{qF}$ with absorption coefficient α corresponding to the different values of recombination velocity S_r.

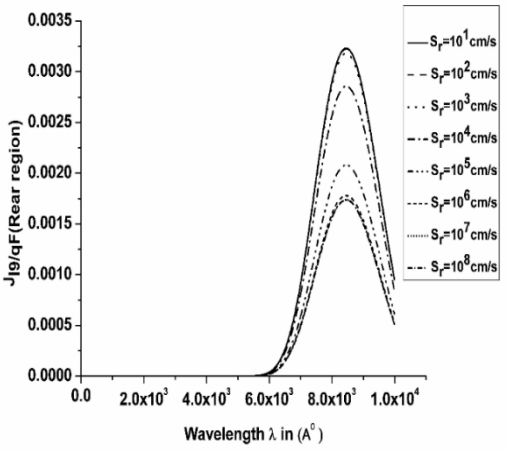

Fig. 10. Variation of $\frac{J_{nl_2}}{qF}$ with wavelength λ corresponding to the different values of recombination velocity S_r.

4. Conclusion

The minority carrier distribution in the front and rear regions of a BESC structure has been investigated and their contributions to the photocurrent of the device has been studied, taking into consideration the front and rear recombination velocities. It is observed that for smaller values of recombination velocities there is improvement in the photocurrent of these structures. This points out the need of a back surface field (BSF) in such devices. Experimental work reported recently has considered similar BSF regions in the new design of such solar cells [8].

Acknowledgements

We are grateful to the Department of Science and Technology, Govt. of India, for financial support under the DST-PURSE Programme, granted to the University of Kalyani. We thank the authorities of the Indian Association for the Cultivation of Science, Kolkata, India, for allowing us to consult their library.

References

[1] D.M. Chapin, C.S. Fuller and G.L. Pearson, "A new silicon p-n junction photocell for converting solar radiation into electrical power", J. Appl. Phys., vol. 25, pp. 676-677, May 1954.

[2] M.B. Prince, "Silicon solar energy converters", J. Appl. Phys.,vol. 26, pp. 534-540, May 1955.

[3] W. Shockley and H.J.Queisser, "Detailed balance limit of efficiency of p-n junction solar cell", J. Appl. Phys., vol. 32, pp. 510-519, 1961.

[4] M.Wolf, "A new look at silicon solar cell performance", Energy Conversion, vol. 11, pp. 63-73, 1971.

[5] A.W. Blakers and M.A. Green,"20% efficiency silicon solar cells",Appl. Phys. Lett.,vol. 48,pp. 215-217, Jan 1986.

[6] W. Wang, J. Zhao and M.A. Green, "24% efficiency silicon solar cells", Appl. Phys. Lett. , vol.57, pp. 602-604, August 1990.

[7] A.S. Bouazzi, M.Abaab and B.Rezig, "A new model of very high efficiency buried emitter silicon solar cell", Solar Energy Materials and Solar Cells, vol. 46, pp. 29-41, 1997.

[8] N.-P. Harder, V. Mertens and R.Brendel, "Buried emitter solar cell structures: Decoupling of metallization geometry and carrier collection geometry of back contacted solar cells", Phys. stat. sol. (RRL), vol. 2, No. 4, pp. 148-150, 2008.

[9] V. Mertens, S. Bordihn, Y. Larionova, N.-P. Harder and R. Brendel, "The buried emittersolar cell concept: Interdigitated Back Junction Structure with virtually 100% emitter coverage of the cell area", 24th European Photovoltaic Solar Energy Conference, Hamburg, Germany, Sept. 2009.

[10] Nils –P. Harder, V. Mertens and R. Brendel, "Numerical simulations of buried emitter back junction solar cells", Prog. Photovolt: Res. Appl., vol. 17, pp.253-263, 2009.